

# Polymesomorphism and orientation in liquid crystalline poly(triethylene glycol *p,p'*-bibenzoate)

Aránzazu Martínez-Gómez · Ernesto Pérez · Antonio Bello

Received: 1 October 2009 / Revised: 17 February 2010 / Accepted: 22 February 2010 / Published online: 20 March 2010  
© Springer-Verlag 2010

**Abstract** The phase transitions and the orientational behavior of liquid crystalline poly(triethylene glycol *p,p'*-bibenzoate) have been studied. The real-time synchrotron diffraction results indicate that, on cooling from the isotropic melt, an orthogonal SmA mesophase is formed first, and later it is transformed into a tilted SmC mesophase. However, the SmA mesophase is stable in a rather wide temperature interval, and the transformation into the SmC phase occurs at temperatures close to the glass transition, so that not very high tilting angles are attained. The uniaxial deformation of the SmC mesophase indicates that usual parallel orientation of the molecular axes in relation to the stretching direction is obtained at high strain rates, while anomalous perpendicular orientation occurs at low deformation rates, with the smectic layers aligned with the stretching direction and the molecular axes almost perpendicular. A mixture of the two types of orientation is observed at intermediate rates, with rather interesting features.

**Keywords** Liquid crystalline polymers (LCP) · Parallel and perpendicular orientation · Smectic mesophases · Synchrotron diffraction · Uniaxial deformation

## Introduction

The phase behavior of liquid crystal polymers (LCPs) is usually rather complicated, and many of these materials exhibit polymorphism and/or polymesomorphism [1, 2]. A

combination of differential scanning calorimetry (DSC) and X-ray diffraction techniques is a very useful tool for the study of the phase behavior. Moreover, taking advantage of the extremely high intensity of synchrotron radiation, very short acquisition times can be used, so that the experiments can be performed under real-time conditions, and temperature programs similar to those employed in DSC can be imposed to the samples. Therefore, both aspects phase transitions and structural information can be determined by real-time variable-temperature diffraction experiments using synchrotron radiation.

Three scattering regions of interest are found in LCPs, characterized by different ranges of the scattering vector,  $q=2\pi/d=4\pi \sin\theta/\lambda$ : (a) the region at higher angles, with a typical  $q$  range between 6 and 25 nm<sup>-1</sup>, designated as wide-angle X-ray scattering (WAXS) region, where the scattering from the amorphous phase, as well as from the smectic and crystalline domains, can be observed. The crystal phases (and the highly ordered smectic crystals) exhibit relatively narrow peaks in the WAXS patterns, overlapped to the amorphous halo. The diffuse scattering in this interval arises either from fully amorphous regions or/and from the diffraction of low-ordered smectic domains in the direction parallel to the smectic layers; (b) a middle-angle X-ray scattering (MAXS) region, covering, approximately, the  $q$  range between 1 and 6 nm<sup>-1</sup>. The mesogenic layer spacing peaks are typically observed in this region; and (c) the small-angle X-ray scattering (SAXS) region, with  $q$  values below 1 nm<sup>-1</sup>. The crystalline long periods, as well as different parameters derived from the correlation function, are obtained from this region [3–5].

In previous works, we have analyzed the liquid crystalline behavior of several semiflexible polybibenzoates [6–17], obtained by polycondensation of mesogenic bibenzoate group with aliphatic diols, finding that the thermotropic

A. Martínez-Gómez (✉) · E. Pérez · A. Bello  
Instituto de Ciencia y Tecnología de Polímeros, CSIC,  
Juan de la Cierva 3,  
28006 Madrid, Spain  
e-mail: aranmg@ictp.csic.es

behavior of these polyesters is strongly conditioned by the nature (chemical structure and even/odd character) of the flexible spacer. For those polymers incorporating linear all-methylene spacers, a rapid transformation of the smectic mesophase into a three-dimensional crystal structure has been found [6, 9, 16, 17]. In contrast, when oxyalkylene spacers are used, this transformation is greatly inhibited [6–8, 15, 17]. This is the case of poly(triethylene glycol *p,p'*-bibenzoate) (PTEB). The mesophase of PTEB is stable for a considerable time although the transformation into a more ordered phase can be attained by annealing for long times at temperatures above the glass transition [17–19]. In previous studies [18, 20], based on DSC experiments and X-ray profiles acquired at room temperature in a conventional diffractometer, the possibility of polymorphism in PTEB was indicated. Furthermore, it was suggested that the temperature of annealing has some effect on the crystalline structure of PTEB.

On the other hand, some LCPs with smectic or nematic mesophases have been reported to exhibit, under particular circumstances of uniaxial stretching or shear deformation, a kind of anomalous orientation where the chain axes are perpendicular to the stretching direction [11, 14, 21–33]. Consequently, the best mechanical properties in such systems are found in the direction normal to the fiber [22], so that new prospects are foreseen from this particular behavior.

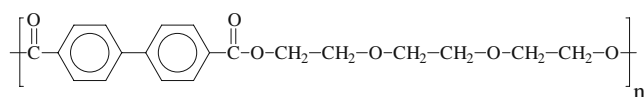
In those reports, nematic or low-ordered smectic mesophases (of the SmA kind, without intralayer correlations of the local tilt directions) were studied. Only in one case [26] the two types of orientation are reported for another polybibenzoate in a mesophase of higher order: a SmC mesophase. However, in that study, the starting points for obtaining the two kinds of orientation are different: the isotropic melt for parallel orientation and the smectic melt for perpendicular one.

The aim of this work is to gain information about the phase behavior of PTEB. A deeper study of this polymer has been carried out by DSC and variable-temperature synchrotron X-ray experiments. In this first paper, the thermotropic behavior of PTEB on cooling from the isotropic melt and during the subsequent heating is analyzed in detail. Moreover, the tensile deformation of its liquid crystalline phase is also analyzed in order to investigate the ability of the SmC mesophase of PTEB to produce the interesting phenomenon of perpendicular orientation, always starting from the same initial state.

## Experimental

PTEB was synthesized in our laboratory by transesterification of dimethyl 1,1'-biphenyl-4,4'-dicarboxylate (Aldrich) with triethylene glycol (Aldrich) using titanium (IV) isopropoxide as catalyst. The polymer was purified by precipitation from a

chloroform solution into methanol. The chemical structure of PTEB:



was confirmed by NMR spectroscopy in deuterated chloroform.

$$\begin{aligned} \delta(^1\text{H NMR}) &= 3.74(\text{s}, 4\text{H}, \text{OCH}_2\text{CH}_2\text{O}), \\ &3.86(\text{t}, 4\text{H}, \text{COOCH}_2\text{CH}_2\text{O}), \\ &4.49(\text{t}, 4\text{H}, \text{COOCH}_2), 7.62(\text{d}, 4\text{H}, \text{OCCCHCHC}), \\ &8.10(\text{d}, 4\text{H}, \text{OCCCHCHC})\text{ppm}. \end{aligned}$$

$$\begin{aligned} \delta(^{13}\text{C NMR}) &= 64.2(\text{COOCH}_2), 69.2(\text{COOCH}_2\text{CH}_2\text{O}), \\ &70.7(\text{OCH}_2\text{CH}_2\text{O}), 127.1 \text{ OCCCHCHC}), \\ &129.5(\text{OCCCHCHC}), 130.2(\text{OCCCHCHC}), \\ &144.3(\text{OCCCHCHC}), 166.2(\text{OCCCHCHC})\text{ppm}. \end{aligned}$$

Weight-average ( $M_w$ ) and number-average ( $M_n$ ) molecular weights and intrinsic viscosity of PTEB were determined by size-exclusion chromatography using a Water Alliance GPCV 2000, equipped with two detectors: the conventional refractive index concentration detector and a viscometer. The dual detection allows to achieve a universal calibration (obtained from measurements in different polystyrene standards, using chloroform as eluent at 35 °C) and to determine absolute molecular weight and viscosity values. The results obtained are  $M_w=18,396$  and  $M_n=9,063$  and an intrinsic viscosity of 0.335 dL g<sup>-1</sup>.

A film of PTEB in the liquid crystalline state was obtained by compression molding in a Collin press between hot plates (135 °C) for 5 min, followed by cooling to room temperature between water-cooled plates. This film was stored in a refrigerator (below the glass transition) in order to prevent the crystallization of the sample.

DSC measurements were performed under nitrogen atmosphere (20 ml min<sup>-1</sup>) in a Perkin-Elmer DSC7 calorimeter, provided with a cooling system. About 6 to 7 mg of the sample was encapsulated in an aluminum pan, and a scanning rate of 8 °C min<sup>-1</sup> was used. The glass transition temperature,  $T_g$ , was taken as the temperature where the specific heat increment is half of the total one at the transition. The transition temperatures were taken as the peak minimum or maximum in the calorimetric curve.

Variable-temperature X-ray diffraction experiments were performed on the Spanish CRG BM16 beamline at ESRF (Grenoble, France). The X-ray beam was monochromatized at the selenium edge ( $\lambda=0.098$  nm). WAXS, MAXS, and SAXS data were collected simultaneously. A MARCCD detector, placed at around 200 cm from the polymer sample and off beam, was able to cover both the SAXS and MAXS

regions (from around 40 to 1.25 nm), while a Princeton detector was used for the WAXS region. A Linkam THMS600 stage was used for controlling the temperature. A scanning rate of  $8\text{ }^{\circ}\text{C min}^{-1}$  was employed. The scattering patterns were collected in time frames of 15 s, so that we have a temperature resolution of  $2\text{ }^{\circ}\text{C}$  between frames. Crystalline iPP and silver behenate samples were used for the calibration of the WAXS and MAXS/SAXS detectors, respectively.

The two-dimensional diffraction patterns were integrated to one-dimensional diffractograms using the FIT2D program of Dr. A. Hammersley of ESRF. Radial integrations of  $360^{\circ}$  of the photographs were done. The profiles were normalized to the primary beam intensity, and the background from the empty sample holder was subtracted. The corresponding profiles represent relative intensity units as a function of the scattering vector.

Oriented fibers were obtained by uniaxial drawing of dumbbell-shaped specimens in a Minimat 2000 dynamometer at  $23\text{ }^{\circ}\text{C}$ , with different crosshead speeds (99, 5, 1, and  $0.2\text{ mm min}^{-1}$ ), up to a final strain of 300%. The specimens for these experiments were punched out from the compression-molded film of PTEB in the liquid crystalline state, so that the starting point is an unaligned multidomain sample. The dimensions of these specimens were 15 mm long, 3 mm wide, and 0.7 mm thick. Actual strain rates were determined from the displacement of parallel ink marks printed 2 mm apart on the specimen prior to drawing.

Wide-angle X-ray diffraction photographs of fibers were taken at  $16\text{ }^{\circ}\text{C}$  (see below) using a flat-plate camera attached to a Phillips 2 kW tube X-ray generator, using nickel-filtered  $\text{CuK}_{\alpha}$  radiation. The distance from sample to the camera film was determined by using aluminum foil as standard. The azimuthal integration of these X-ray photographs was performed in a narrow range of scattering vector around both the smectic layer spacing and the wide-angle amorphous-like halo. The origin for the azimuthal angle,  $\alpha$ , has been taken in the equator (fiber direction in the meridian).

## Results and discussion

### Thermal properties and phase behavior

Figure 1 shows the DSC curves corresponding to PTEB in a cooling–heating experiment at  $8\text{ }^{\circ}\text{C min}^{-1}$ . On cooling from the isotropic melt (bottom curve), an exothermic peak at  $106\text{ }^{\circ}\text{C}$ , with an enthalpy of  $10.4\text{ J g}^{-1}$ , and a glass transition at  $8\text{ }^{\circ}\text{C}$  are clearly observed. The subsequent heating of the sample (top curve) presents again the glass transition, centered at  $11\text{ }^{\circ}\text{C}$ , and an endothermic peak at  $115\text{ }^{\circ}\text{C}$ , with an enthalpy of  $10.7\text{ J g}^{-1}$ . The low undercooling and the magnitude of the enthalpy are indicative of the formation of

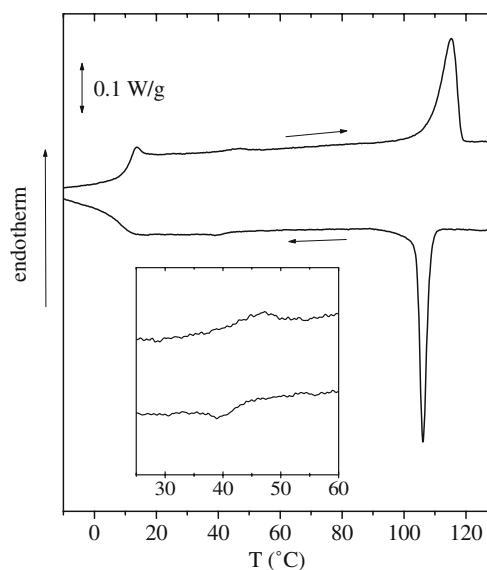


**Fig. 1** DSC curves corresponding to PTEB in the cooling from the isotropic melt (*lower*) and the subsequent heating (*upper*). Scanning rate  $8\text{ }^{\circ}\text{C min}^{-1}$

a low-ordered mesophase. Moreover, one can see that a very weak transition is detected at lower temperatures (see insert), at  $40\text{ }^{\circ}\text{C}$  in the cooling curve, and at  $47\text{ }^{\circ}\text{C}$  in the heating curve.

A detailed study of the phase behavior of PTEB has been carried out by variable-temperature X-ray experiments by employing synchrotron radiation. The MAXS/WAXS profiles acquired during a cooling/heating experiment similar to that in DSC are shown in Figs. 2 and 3. In the cooling experiment from the isotropic melt (Fig. 2), the patterns at high temperatures only show the amorphous WAXS halo associated with the averaged intermolecular distance of polymer chains in the isotropic melt. On lowering the temperature, at  $110\text{ }^{\circ}\text{C}$ , the MAXS region shows the appearance of a sharp peak at  $q=3.2\text{ nm}^{-1}$  ( $d=1.96\text{ nm}$ ), and its intensity increases quickly while the WAXS halo undergoes a narrowing and a slight

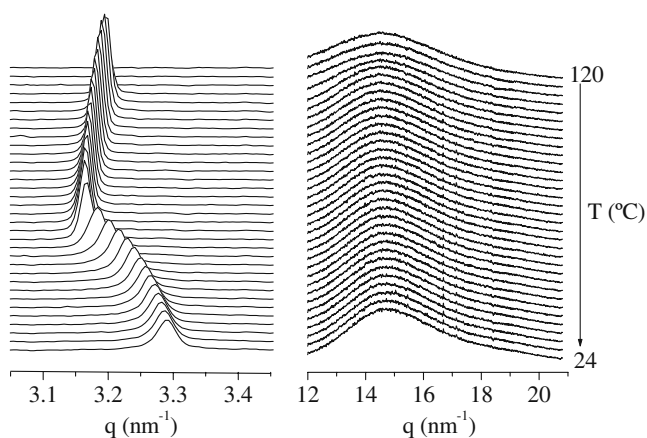


**Fig. 2** MAXS/WAXS synchrotron profiles for PTEB on cooling from the isotropic melt. For clarity, only one of every two frames is plotted. Scanning rate  $8\text{ }^{\circ}\text{C min}^{-1}$

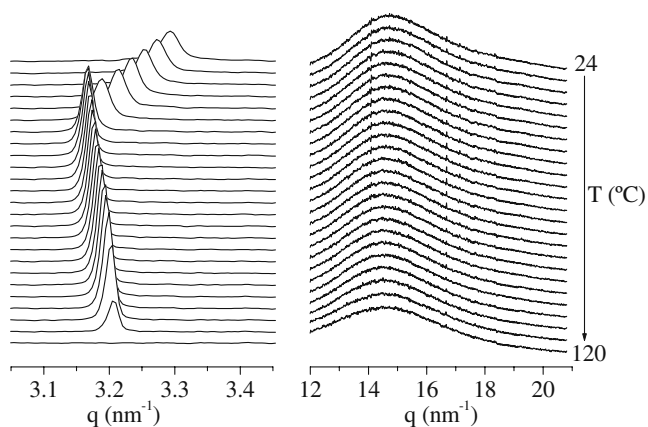


**Fig. 3** MAXS/WAXS synchrotron profiles corresponding to a freshly cooled PTEB sample in a heating experiment. For clarity, only one of every two frames is plotted. Scanning rate  $8\text{ }^{\circ}\text{C min}^{-1}$

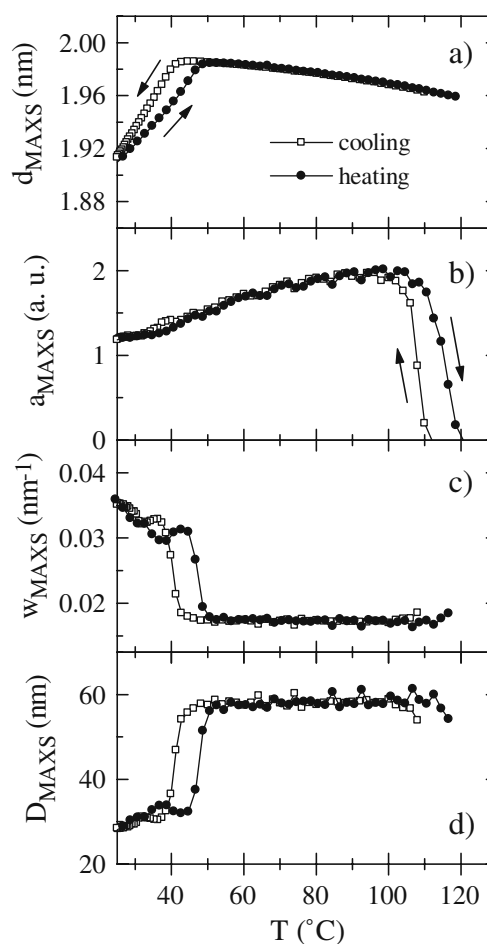
change in its maximum position, suggesting a decrease of the averaged intermolecular distances. These features indicate the formation of a low-ordered smectic mesophase, with a smectic layer spacing of 1.96 nm and the absence of lateral order within the layers. By further decreasing the temperature below  $40\text{ }^{\circ}\text{C}$ , it is observed that the MAXS peak shifts to higher  $q$  values (lower spacings), while the peak loses intensity and becomes wider. On the other hand, no changes are observed in the amorphous-like WAXS halo, with the exception of a slight linear decrease of its position due to the thermal contraction.

A detailed analysis of the variation with temperature of the MAXS peak parameters (position, area, and intensity) has been carried out in these diffractograms, and the results are presented in Figs. 4 and 5. As it is seen in Fig. 4a, the temperature dependence of the smectic layer spacing,  $d_{\text{MAXS}}$ , shows two clear regions: (a) from its appearance at  $110\text{ }^{\circ}\text{C}$  (in accordance with the exothermic DSC peak) down to about  $40\text{ }^{\circ}\text{C}$  and (b) below  $40\text{ }^{\circ}\text{C}$ . In the first region,  $d_{\text{MAXS}}$  is close to the length of the extended [8] repeating unit of PTEB, indicating that a SmA mesophase is first formed. In the second region, at temperatures below  $40\text{ }^{\circ}\text{C}$ , the smectic spacing decreases clearly with temperature, from 1.98 nm to a value of 1.91 nm at  $24\text{ }^{\circ}\text{C}$ . This reduction of the smectic spacing with decreasing temperature can be interpreted as a tilting of the smectic structure leading to a SmC mesophase [10, 12, 34]. Furthermore, it is observed that the smectic peak loses intensity and becomes wider in such a way that the area of the peak is practically unaffected (Fig. 4b). It should be noted that while a continuous shifting of the smectic spacing takes place during the temperature interval between  $40\text{ }^{\circ}\text{C}$  and  $24\text{ }^{\circ}\text{C}$ , a clear discontinuity is detected for the width and height of the MAXS peak at the beginning of the SmA–SmC transition (see Figs. 4c and 5a).

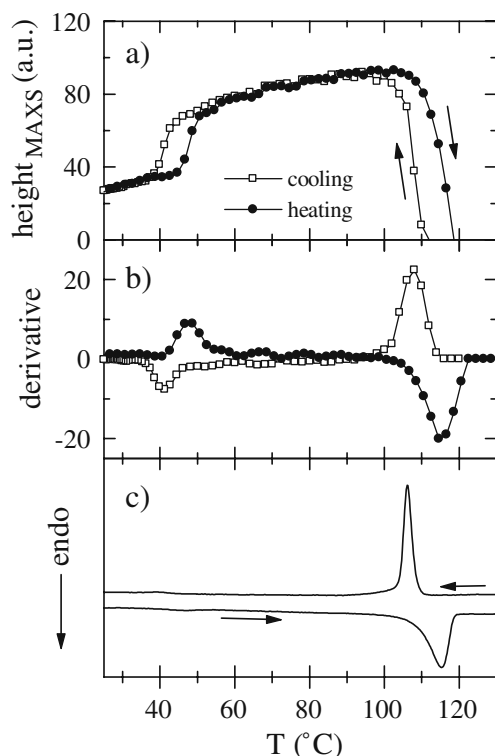
Therefore, the width or the height of the MAXS peak is a good monitor of the phase transitions. Thus, as shown in

Fig. 5b, the derivative of peak height in the cooling experiment shows two peaks, centered at  $41\text{ }^{\circ}\text{C}$  and at  $108\text{ }^{\circ}\text{C}$ , in good agreement with the exothermic peaks detected in the DSC experiment (Figs. 1 and 5c). But now the subtle DSC transition at around  $40\text{ }^{\circ}\text{C}$  is much better observed.

The width of the layer peak also shows a rather important change at the transition. The correlation length,  $D_{\text{MAXS}}$ , of the smectic domains along the layer normal can be estimated from such width. The results are presented in Fig. 4d, showing an abrupt decrease when the SmC phase is formed. Thus, values around 58 nm are deduced for the SmA mesophase, while only around 30 nm are found after the transition. The implication is that the longitudinal long range order is considerably higher in the SmA phase: Since the layers must continually break and reform as they tilt with respect to the molecular axes, the long-range order in the SmC phase is worse than the corresponding one in the SmA phase, as previously reported [35]. Evidently, this loss of longitudinal order in the SmC mesophase is accompanied by formation of intralayer correlations of the local tilt directions, so that SmC



**Fig. 4** Temperature dependence of different parameters for the smectic layer diffraction: **a** layer thickness, **b** area, **c** width at half-height, and **d** correlation length, corresponding to PTEB in the synchrotron experiments of Figs. 2 and 3



**Fig. 5** Variation of **a** the height of the MAXS peak and **b** its derivative as a function of temperature. The DSC curves are presented in the lower part of the figure (**c**), for comparison

mesophases display an overall degree of order higher than that for the SmA ones.

Therefore, the sequence of phases: Isotropic melt–SmA–SmC is observed by cooling PTEB. Moreover, the mesophase of PTEB is not transformed into a three-dimensional crystalline phase (as it happens with polybibenzoates with linear all-methylene spacers) at the usual cooling rates in the calorimeter.

Since highly ordered structures are not involved in these experiments, the SAXS region is of very little information, so that this region is not shown in Figs. 2 and 3.

It is also important to notice that the thermal stability of the SmA mesophase of PTEB is considerably higher than that observed for other polybibenzoates, where the SmC–SmA transition takes place shortly after the SmA formation [10, 12]. As shown in Fig. 4a, the SmA mesophase of PTEB is stable in a rather wide temperature interval. Moreover, it is observed that the layer thickness shows a slight increase with decreasing temperature. The temperature coefficient takes a value of  $(-4 \pm 1) \times 10^{-4} \text{ nm K}^{-1}$ . Negative coefficients have already been reported in other smectic polybibenzoates [12, 16, 36, 37]. The interpretation is that the thermal contraction expected in a certain dimension on cooling is counterbalanced by an increasing degree of orientational order that the SmA phase experiences on cooling [38] and/or by gauche–trans conformational transitions in the flexible spacer.

The synchrotron diffractograms during the heating of a freshly cooled sample of PTEB (Fig. 3) show the inverse sequence of phases: SmC–SmA–isotropic melt. The variation with temperature of the MAXS peak parameters is also displayed in Figs. 4 and 5. It is seen that the SmA phase is reached at around 48 °C, and in the interval 24–48 °C, the layer thickness continuously shifts to higher spacings, from 1.91 to 1.98 nm, showing also an increase of its intensity and becoming narrower when the SmA structure is finally achieved. Thus, the correlation length increases rather sharply from around 30 nm in the SmC mesophase to a value of around 58 nm after transformation into the SmA phase (Fig. 4d).

Moreover, the derivative of the MAXS peak height shows a maximum at 48 °C (Fig. 5b) that matches the location of the weak endotherm detected in the heating DSC curve. Finally, in accordance with the endothermic DSC peak at 115 °C, another maximum appears at 116 °C in the derivative of the height, and the isotropization of the SmA mesophase is attained at 120 °C: The MAXS peak has completely disappeared and an amorphous halo is observed in the WAXS region.

According to the Landau–de Gennes theory, the transition from SmA to SmC mesophase can be described by the continuous increase of the tilt angle,  $\theta$  (taken as the order parameter of the transition), in such a way that the free energy can be expressed in terms of powers of the tilt angle [39]. In such case and neglecting the higher powers of  $\theta$ , i.e., for temperatures not far away from the temperature at which the tilt appears,  $T_c$ , the following equation is obtained:

$$\theta = k(T_c - T)^{0.5} \quad (1)$$

where  $k$  is a constant. The tilt angle  $\theta$  can be estimated indirectly from the reduction of the smectic spacing using the expression:

$$\cos \theta = d_\theta / d_0 \quad (2)$$

where  $d_\theta$  is the smectic spacing of the SmC mesophase at different temperatures and consequently at different tilt angles and  $d_0$  is the smectic spacing for a tilt angle equal to zero (SmA mesophase). Considering that  $d_0$  is 1.98 nm for PTEB, the variation with temperature of the tilt angle has been displayed in Fig. 6. It can be seen that the present data are fitted rather well, in the whole temperature interval, to a parabolic function of the type of Eq. 1, with  $k=3.85$  and  $T_c=41.5$  °C and  $k=3.35$  and  $T_c=48.7$  °C for the cooling and heating experiments, respectively. Moreover, it is observed that a tilt angle of only 16° is finally attained, a value considerably smaller than those reported for SmC mesophases in other polybibenzoates [10, 12] (around 30°). One of the possible reasons is that our synchrotron experiments only allow us to detect the high-temperature region of the tilting

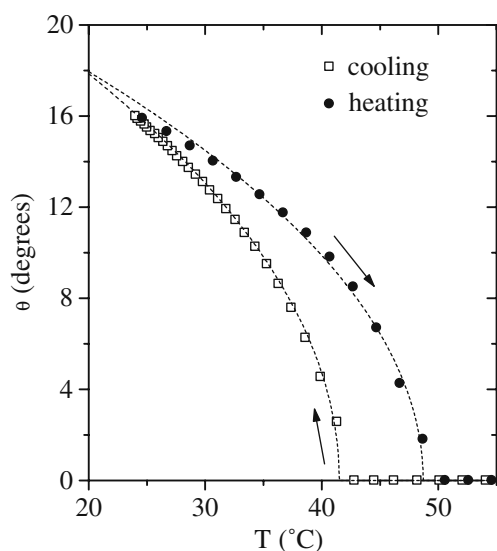


**Fig. 6** Temperature dependence of the tilt angle of the SmC mesophase of PTEB. The *dashed lines* correspond to the fitting to Eq. 1, with the parameters indicated in the text

associated to the SmA–SmC transition in PTEB since the complete development would happen at temperatures lower than ambient temperature. Nevertheless, the proximity of the glass transition (see Fig. 1) will prevent, most probably, the attainment of much higher angles of tilting.

**Mechanical properties: parallel and perpendicular orientation**

The mechanical properties of liquid crystalline PTEB (in the SmC mesophase) have been evaluated from stress–strain experiments at different stretching rates. The effect of strain rate on the molecular orientation has also been investigated. Figure 7 shows the stress–strain curves obtained at 23 °C with different crosshead speeds. The curve corresponding to the highest rate (99 mm min<sup>-1</sup>) shows three regions: an initial elastic region, a clearly marked yield point related to the development of the neck, followed by cold-drawing (propagation of the neck) and a final strain-hardening region. Although we are dealing with a low-ordered smectic mesophase, the shape of this stress–strain curve resembles that for semicrystalline polymers (except for the rather low values of the stress).

The stress–strain curves at slower deformation speeds show that the yield process becomes increasingly delocalized and diffuse. It is also seen that the strain-hardening effect is not observed. This mechanism of deformation is similar to that of an elastomer: The deformation occurs in a macrohomogeneous way without the formation and growth of a neck.

From these curves, different mechanical parameters can be estimated, namely the stiffness of the polymer, measured by the initial slope of the stress–strain curve, and the yield

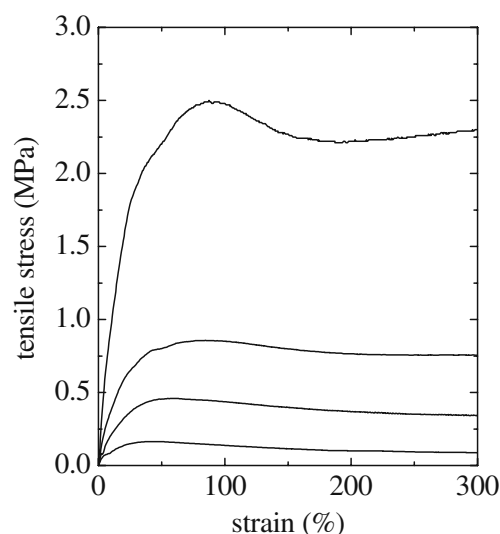


**Fig. 7** Stress–strain curves corresponding to the uniaxial stretching of liquid crystalline specimens of PTEB at 23 °C with different crosshead speeds (from *bottom to top* 0.2, 1, 5, and 99 mm min<sup>-1</sup>)

strength. The tensile modulus and yield strength values are shown in Table 1. It can be observed that the two magnitudes are decreasing functions of the stretching rate.

The 2D X-ray photographs for the PTEB fibers obtained at the end of these stress–strain experiments (after a few minutes of relaxation with fixed ends) are shown in Fig. 8. The photographs were acquired at 16 °C, a temperature low enough in order to prevent the crystallization [17–20] of PTEB during the acquisition of the photo (around 2 h). The four diffractograms show a broad amorphous-like diffraction at high angles and narrow diffractions, corresponding to the smectic layer spacing, at lower angles. The photograph at the bottom, corresponding to the fiber stretched at 99 mm min<sup>-1</sup> (actual strain rate of 1,800% min<sup>-1</sup>), is characteristic of a SmC mesophase [40] since the smectic layer reflection is split at both sides of the meridian (fiber direction) while the broad wide-angle diffractions are centered on the equator. Therefore, at high strain rate, the molecular axes (and the director) are aligned with the elongation direction, as corresponds to a usual parallel orientation.

The photograph for the lowest strain rate, 3% min<sup>-1</sup>, looks completely different: The smectic layer diffractions are centered on the equator, and it seems that the broad

**Table 1** Tensile modulus and yield strength for liquid crystalline PTEB stretched at 23 °C with different crosshead speeds

Speed (mm/min)	Tensile modulus (MPa)	Yield strength (MPa)
99	0.13	2.5
5	0.05	0.86
1	0.02	0.46
0.2	0.01	0.16

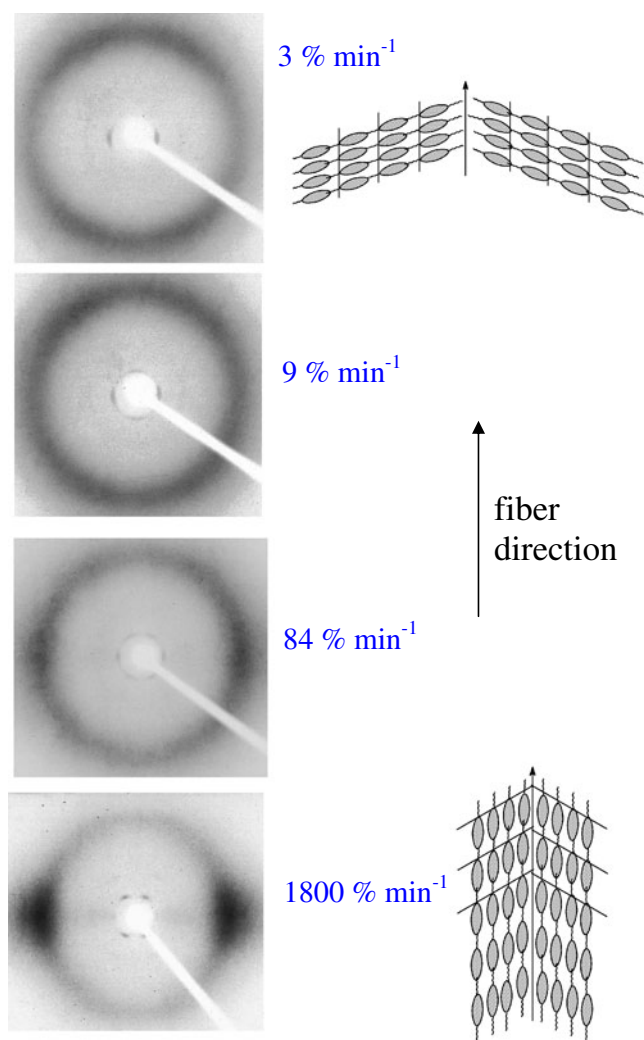


**Fig. 8** X-ray photographs, acquired at 16 °C, of the fibers after uniaxial stretching of liquid crystalline specimens of PTEB at 23 °C and with the indicated actual strain rates. Fiber direction: *vertical*. The proposed molecular arrangements for the parallel (*bottom*) and perpendicular (*top*) orientations are also sketched

wide-angle diffractions are split on both sides of the meridian. Therefore, an anomalous orientation is deduced since the smectic layers are now parallel to the stretching direction and the molecular axes are almost perpendicular.

More information about the molecular arrangement in these fibers can be obtained from the azimuthal integration of the 2D X-ray photographs. The origin for the azimuthal angle,  $\alpha$ , has been taken in the equator. The results obtained for the integration in the region of the smectic spacing and of the wide-angle halo are presented in Fig. 9. All the curves show a minimum at around  $-45^\circ$  due to the presence of the beam stop holder. As commented above, parallel orientation of the molecular axes (and the director) in relation to the stretching direction is observed for the highest deformation rate. Thus, the distribution curve of the smectic peak shows four maxima, the second one somewhat

covered by the beam stop holder minimum. From the maxima at azimuthal angles of  $61^\circ$  and  $119^\circ$ , it is deduced that a tilt angle of around  $29^\circ$  is formed between the normal to the smectic planes and the stretching direction. On the other hand, the curve obtained in the analysis of the wide-angle halo shows two maxima at  $0^\circ$  and  $180^\circ$ . This is indicative of a parallel orientation of the molecular axes with the elongation direction. The molecular arrangement in this fiber is illustrated at the right of the corresponding photograph in Fig. 8.

The fiber obtained at the lowest rate shows a very different behavior. Two maxima centered at  $0^\circ$  and  $180^\circ$  are found for the MAXS spacing, indicating that the smectic layers lie parallel to the stretching direction (molecular axes almost perpendicular), and the distribution curve corresponding to the wide-angle diffractions shows four maxima shifted around  $\pm 20^\circ$  from the fiber direction (the meridian, with  $\alpha=90^\circ$ ). This fact suggests that the macromolecules are oriented forming an angle of  $\pm 20^\circ$  with the perpendicular to the elongation

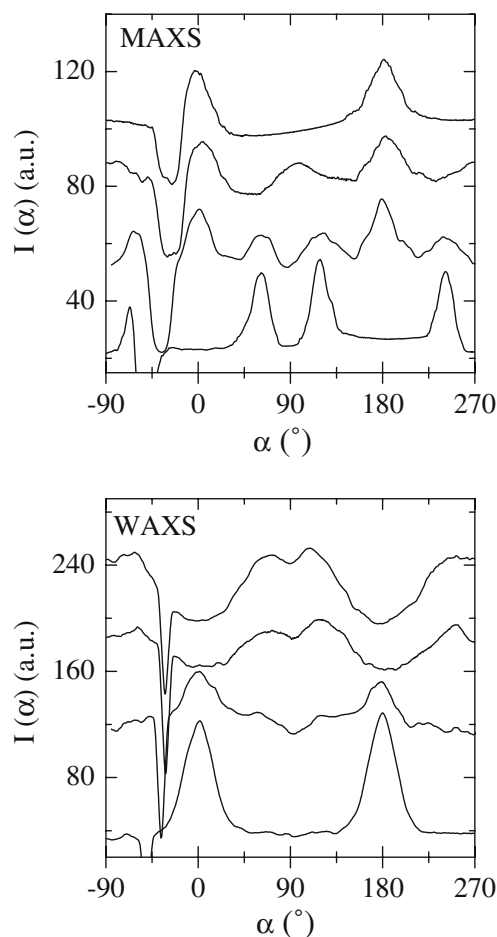


**Fig. 9** Results for the azimuthal integration in the region of the smectic layer reflection (*upper*) and of the wide-angle amorphous-like halo (*lower*) of the X-ray photographs of PTEB fibers in Fig. 8. The origin for the azimuthal angle  $\alpha$  has been taken in the equator. The curves are shifted vertically for clarity (from *top* to *bottom* 3%, 9%, 84%, and 1,800%  $\text{min}^{-1}$ , respectively)

direction. A possible molecular arrangement in this fiber is illustrated in Fig. 8.

Evidently, as deduced from the diffractograms, this structure is not just a rotation by  $90^\circ$  of the one for parallel orientation. Now, the normal to the smectic planes is the direction strictly perpendicular to the stretching direction, so that the layer diffraction spots lie in the equator. On the contrary, the molecular axes are tilted around  $\pm 20^\circ$ , this alternation giving rise to the splitting of the WAXD broad peak. Anyway, the molecular axes are almost perpendicular to the stretching direction.

It is interesting to note that for these very low deformation rates, the width of the peaks after azimuthal integration in the MAXS region is considerably higher than that for the highest rate (see Fig. 9), indicating that the order parameters attained for the perpendicular orientation are significantly smaller than for the pure parallel case. It has been reported [40] that, for low molar mass LCs under a weak aligning field, the SmC diffraction patterns are aligned with the meridian and the WAXS region may present diffuse peaks above and below the equator. This seems to be the situation in our case, with the obvious important difference that now perpendicular orientation is obtained, so that the MAXS peaks lie on the equator and the WAXS diffuse peaks are at both sides of the meridian.

A mixture of parallel/perpendicular orientation is developed when intermediate strain rates are used. As observed in the fiber obtained at  $84\% \text{ min}^{-1}$ , the smectic peak intensity is concentrated in six spots: Two spots are located on the equator at  $0^\circ$  and  $180^\circ$ , as in the fiber at the lowest strain rate (perpendicular orientation), and four spots are split at both sides of the meridian, as in the fiber stretched at high strain rate (parallel orientation).

Finally, it is interesting to note that for the slower rates at which a mixed behavior is obtained, a different orientation of the smectic diffractions associated with the parallel component is found. As an example, the fiber stretched at  $9\% \text{ min}^{-1}$  is shown in Fig. 8. It is observed that the smectic spots corresponding to the parallel orientation do not appear split, but they are centered on the meridian. Consequently, four peaks are observed in the curve after azimuthal integration of the MAXS diffractions, centered at angles of  $0^\circ$ ,  $90^\circ$ ,  $180^\circ$ , and  $270^\circ$ . The WAXS region, however, does not allow distinguishing if the diffuse peak corresponding to parallel orientation is split above and below the equator, due to the low amount of material with parallel orientation (and the presence of perpendicular one), and if we want to increase such amount, higher deformation rates are needed, which lead to the typical four-spot pattern in the MAXS region.

Recently, the orientational behavior of a smectic polybenzoate [25] was studied by real-time simultaneous synchrotron X-ray diffraction and stress–strain experiments. It was found that during the elastic zone and around the

yielding point, exclusively anomalous perpendicular orientation is attained, with the molecular axes perpendicular to the uniaxial deformation direction. However, at the end of the necking region and the beginning of the strain-hardening process, parallel orientation begins to be obtained and its intensity increases with the strain hardening, provided that the stretching conditions are such to develop parallel orientation, i.e., at high strain rates and/or low deformation temperatures. Other works [14, 21–24], based on nonreal-time experiments, have shown that the final proportion of the two kinds of orientations (parallel and perpendicular) in the fiber depends very much on the stretching conditions (temperature and rate of deformation) and also on the molecular weight.

A model for the two kinds of orientation, based on the hierarchical structure of liquid crystalline polymers, has been proposed [23]. In that model, the initial structure of the smectic polybenzoates can be envisaged as composed of domains randomly oriented but with a rather uniform order parameter inside the domains. If it is assumed that the dimensions of the domain in the lateral direction are considerably larger than in the direction of the molecular axis, it seems reasonable to expect that in the case of low strain rates and/or high deformation temperatures, these domains will be able to slide through the disclinations and reorient in the direction of deformation, ending with the largest dimension oriented with the deformation, so that the molecular axes are perpendicular to the stretching direction. On the contrary, in the case of high strain rates and/or low temperatures, the domains will not be able to follow the deformation and, presumably, they will broke apart and reorganize into some kind of fibrillar structure, ending with the molecular axes parallel to the direction of deformation. This model for parallel orientation is similar to that proposed for the deformation of semicrystalline polymers [41, 42], where the initial lamellar crystals, through chain tilting, slip and breaking off, and subsequent re-formation of domains, lead to a fiber formation, oriented along the stretching direction.

In the present work, it has been shown that the SmC mesophase of PTEB polymer follows these orientation pathways. Parallel orientation of macromolecules is obtained at high strain rates while perpendicular orientation is achieved at very low strain rates. In the fiber with parallel orientation, the macromolecular axes are aligned in the fiber direction and the SmC structure is formed by a tilting of the smectic layers. However, the perpendicular orientation of this mesophase arranges the smectic planes parallel to the deformation direction and the polymer chains tilted around  $20^\circ$  from its perpendicular direction.

As a final remark, the present paper is a step further in relation to previous works since here we are studying the orientational behavior under deformation in a mesophase of a higher degree of order: a SmC mesophase with intralayer correlations of the local tilt directions. In principle, the



orientational behavior will depend very much on the degree of order of the phase in question, and it is expected to have a very important influence on the final properties (mechanical, optical, etc.). Its study is, therefore, of capital importance. In this context, our next objective is to study such behavior in mesophases with even higher degrees of order.

## Conclusions

The real-time synchrotron diffraction results in a sample of PTEB indicate a very interesting polymesomorphism for this polymer. Thus, on cooling from the isotropic melt, an orthogonal SmA mesophase is formed first, and later it is transformed into a tilted SmC mesophase. However, the SmA mesophase is stable in a rather wide temperature interval, and the transformation into the SmC phase occurs at temperatures close to the glass transition, so that not very high tilting angles are attained. A reverse phase sequence is observed in the subsequent melting, all the transition temperatures being in very good agreement with the DSC results.

The uniaxial deformation of the SmC mesophase, performed at low temperatures in order to prevent the formation of three-dimensional crystalline structures, indicates that normal parallel orientation of the molecular axes is obtained at high strain rates, while anomalous perpendicular orientation occurs at low deformation rates. However, the corresponding diffractograms (and structures) are not just a rotation by 90° from one to another. A mixture of the two types of orientation are observed at intermediate rates, with rather interesting features since up to six spots are observed in the MAXS region of the layer spacing.

It is important to note that in all deformation experiments, the starting point is the same—the SmC mesophase—and only the strain rate is changed.

**Acknowledgments** We acknowledge the financial support of MICIIN, Projects MAT2007-65519-C02-01 and MAT2007-65519-C02-02. The synchrotron work was also supported by MICIIN through specific grants for the access to the CRG beamline BM16 of the ESRF. The inestimable help of all the beamline personnel is also gratefully acknowledged.

## References

- Nöel C, Narvard P (1991) *Prog Polym Sci* 16:55–110
- Finkelmann H, Rehage G (1984) *Adv Polym Sci* 60/61:97–172
- Vonk CG (1973) *Appl Cryst* 6:81–86
- Goderis B, Reynaers H, Koch MHJ, Mathot VBFJ (1999) *J Polym Sci Part B Polym Phys* 37:1715–1738
- Strobl GT, Schneider MJ (1980) *J Polym Sci Part B Polym Phys* 18:1343–1359
- Pérez E, Pereña JM, Benavente R, Bello A (1997) In: Cheremisinoff NP (ed) *Handbook of engineering polymeric materials*. Marcel Dekker, New York, pp 383–397
- Bello A, Pérez E, Marugán MM, Pereña JM (1990) *Macromolecules* 23:905–907
- Pérez E, Riande E, Bello A, Benavente R, Pereña JM (1992) *Macromolecules* 25:605–610
- Pérez E, Zhen Z, Bello A, Benavente R, Pereña JM (1994) *Polymer* 35:4794–4798
- Pérez E, del Campo A, Bello A, Benavente R (2000) *Macromolecules* 33:3023–3030
- Bello P, Bello A, Riande E, Heaton NJ (2001) *Macromolecules* 34:181–186
- Martínez-Gómez A, Bello A, Pérez E (2004) *Macromolecules* 37:8634–8640
- Martínez-Gómez A, Bello A, Pérez E (2008) *e-Polymers* 69:1–26
- Fernández-Blázquez JP, Bello A, Pérez E (2007) *Macromol Chem Phys* 208:2611–2620
- Pérez E, Benavente R, Cerrada ML, Bello A, Pereña JM (2003) *Macromol Chem Phys* 204:2155–2162
- Pérez E, Todorova G, Krasteva M, Pereña JM, Bello A, Marugán MM, Shlouf M (2003) *Macromol Chem Phys* 204:1791–1799
- Bello A, Pereña JM, Pérez E, Benavente R (1994) *Macromol Symp* 84:297–306
- Benavente R, Pereña JM, Pérez E, Bello A (1994) *Polymer* 35:3686–3690
- Martínez-Gómez A, Pérez E, Álvarez C (2009) *Polymer* 50:1447–1455
- Pérez E, Benavente R, Bello A, Pereña JM, VanderHart DL (1995) *Macromolecules* 28:6211–6218
- Bello P, Bello A, Lorenzo V (2001) *Polymer* 42:4449–4452
- Martínez-Gómez A, Pereña JM, Lorenzo V, Bello A, Pérez E (2003) *Macromolecules* 36:5798–5803
- Fernández-Blázquez JP, Bello A, Pérez E (2007) *Macromolecules* 40:703–709
- Rodríguez-Amor V, Fernández-Blázquez JP, Bello A, Pérez E, Cerrada ML (2008) *Polym Bull* 60:89–96
- Fernández-Blázquez JP, Bello A, Cerrada ML, Pérez E (2008) *Macromolecules* 41:421–428
- Tokita M, Osada K, Kawauchi S, Watanabe J (1998) *Polym J* 30:687–690
- Tokita M, Tokunaga K, Funaoka S, Osada K, Watanabe J (2004) *Macromolecules* 37:2527–2531
- Osada K, Koike M, Tagawa H, Hunaoka S, Tokita M, Watanabe J (2005) *Macromolecules* 38:7337–7342
- Leland M, Wu Z, Chhajer M, Ho R-M, Cheng SZD, Keller A, Kricheldorf HR (1997) *Macromolecules* 30:5249–5254
- Ugaz VM, Burghardt WR (1998) *Macromolecules* 31:8474–8484
- Zhou W-J, Kornfield JA, Ugaz VM, Burghardt WR, Link DR, Clark NA (1999) *Macromolecules* 32:5581–5593
- Romo-Urbe A, Windle AH (1993) *Macromolecules* 26:7100–7102
- Romo-Urbe A, Windle AH (1996) *Macromolecules* 29:6246–6255
- Watanabe J, Hayashi M, Nakata Y, Niori T, Tokita M (1997) *Prog Polym Sci* 22:1053–1087
- Ocko BM, Kortan AR, Birgeneau RJ, Goodby JW (1984) *J Phys France* 45:113–128
- Todorova GK, Krasteva MN, Pérez E, Pereña JM, Bello A (2004) *Macromolecules* 37:118–125
- Ressia JA, Quinzani LM, Valles EM, Bello P, Bello A (2004) *Mol Cryst Liq Cryst* 420:9–33
- Lagerwall JPF, Giesselmann F (2006) *Chem Phys Chem* 7:20–45
- Lagerwall ST (1999) *Ferroelectric and antiferroelectric liquid crystals*. Wiley, New York
- Seddon JM (1998) In: Demus D, Goodby J, Gray GW, Spiess HW, Vill V (eds) *Handbook of liquid crystals*, vol 1. Wiley, Weinheim, pp 635–679
- Alexander LE (1969) *X-ray diffraction methods in polymer science*. Wiley, New York
- Peterlin A (1966) *Structure of drawn polymers*, technical report AFML-TR-67-6. USAF Material Laboratory, Wright-Patterson, AFB